Available online at www.sciencedirect.com
SCIENCE DIRECT
Sensors and Actuators B 114 (2006) 254–262
SENSORS AND ACTUATORS B CHEMICAL
www.elsevier.com/locate/snb

Compliant and low-cost humidity nanosensors using nanoporous polymer membranes

Bozhi Yang, Burak Aksak, Qiao Lin, Metin Sitti *

Department of Mechanical Engineering, Carnegie Mellon University, Pittsburgh, PA 15213, USA

Received 28 December 2004; received in revised form 5 May 2005; accepted 20 May 2005
Available online 1 August 2005

Abstract

This paper proposes non-fragile compliant humidity nanosensors that can be fabricated inexpensively on various types of nanoporous polymer membranes such as polycarbonate, cellulose acetate, and nylon membranes. The nanosensor contains a pair of interdigitated electrodes deposited on the nanoporous polymer membranes. The resistance and/or capacitance between these electrodes vary at different humidity levels with a very high sensitivity due to the water adsorption (capillary condensation) inside the nanopores. The proposed sensors are low-cost in both material and fabrication. Due to its compliance, the sensors can be suitable for certain applications such as in situ water leakage detection on roofs, where people can walk on top of them. Testing results demonstrated that the sensor changes resistance within large range of relative humidity (RH) values (40–100% RH) with very high sensitivity. Design A and B sensors exhibit high sensitivities, 2.5 and 1.3 GΩ/% RH, respectively, to relative humidity changes but are not linear in response till 55% RH is reached ($R^2 \sim 0.7391$ for design A, $R^2 \sim 0.8824$ for design B). For the design C sensors, sensitivity is around 20 GΩ/% RH and the response is highly linear ($R^2 \sim 0.96$) for 40–100% relative humidity range. These results showed the feasibility of the proposed compliant and low-cost nanopore polymer membrane based humidity nanosensors which could be used for in situ water leakage and humidity level detection on three-dimensional and complex surfaces such as roofs and airplane bodies in the near future.

Keywords: Nanosensors; Humidity sensors; Nanoporous membranes

1. Introduction

Humidity sensors are important for a wide range of applications such as meteorological services, air conditioning, and electronics processing [1]. Based on the sensing principle used, the most common humidity sensors are resistive and capacitive humidity sensors. Resistive humidity sensors usually consist of an interdigitated metal electrode on a moisture-sensitive substrate such as porous ceramic [2]. The devices' resistance varies exponentially with variations in relative humidity. On the other hand, capacitive humidity sensors are based on non-conducting materials, which make up the dielectric of a capacitor. The dielectric constant of the film changes as it absorbs water vapor, varying the sensors capacitance in proportion to the changes in relative humidity [3–7].

Nanopore based humidity nanosensors can detect the resistance and/or capacitance change with a very high sensitivity due to water adsorption (capillary condensation) inside the nanopores which have very high surface area-to-volume ratio [1]. Depending on the relative humidity levels of the environment where the nanosensor will be used, the pore size can be determined such that it will give the highest sensitivity for the operating range [8]. In literature, there are many works related to using alumina and other ceramic nanopore materials for humidity sensing [1,9]. However, ceramic humidity sensors suffer from insufficient sensitivity, low reversibility, and drift in base resistance with time [10]. In addition, the brittleness makes ceramics not suitable for certain applications such as in situ water leakage detection on roofs where people can walk on top of them. Another common sensor material,

* Corresponding author.
E-mail address: sitti@cmu.edu (M. Sitti).

0925-4005/$ – see front matter © 2005 Elsevier B.V. All rights reserved.
doi:10.1016/j.snb.2005.05.017

polyimide film with roughened surface, has been widely used [11–17]. But it swells with water absorption and has a relatively lower sensitivity. Therefore, in this work, novel compliant and nanoporous polymer materials are proposed as sensing materials for non-fragile and high sensitivity humidity sensing. Resistive sensing is used for the measurements due to its simplicity and easy integration to the nanosensor for miniature sensor networks/arrays in the future.

2. Sensing materials and mechanism

Polycarbonate (PC), cellulose acetate (CA) and polyester (nylon) membranes with nanopores were utilized as the sensing materials and their performances are compared. Fig. 1 shows the scanning electron microscope (SEM) images of the PC and nylon membranes that we used. Table 1 shows the properties of these membranes.

All of the three materials are commercially available as inexpensive thin 25 mm diameter circular membranes. The PC, CA, and nylon membranes have a pore size of 200, 200, and 100 nm, respectively. The pore density is 3×10^8 pores/cm^2 for PC membrane, and the porosity is 66% and 50% for CA and nylon membrane, respectively. Interdigitated gold electrodes were fabricated on top of these membranes, and resistance and/or capacitance change of the nanosensor was measured between the electrodes under different humidity conditions. All the membranes are commercially available and obtained from Advantec MFS, Inc., Dublin, CA.

The ability of a porous membrane to sense humidity is based upon ionic conduction [10]. The presence of an adsorbed layer of water at the surface reduces the total sensor impedance due to the increase in the ionic conductivity, as well as the capacitance due to the high dielectric constant of water. An additional advantage of porosity is that at a particular temperature and relative humidity (RH), water condensation occurs in pores up to r in radius given by Kelvin's relation [10]:

$$r\,(\mathrm{nm}) = \frac{2\gamma_L V}{RT\log(P/P_s)} \approx \frac{1.08}{\log(P/P_s)}$$

where P/P_s is the relative humidity, γ_L the water surface tension, R the universal gas constant, T the temperature in K, and V is the volume of water. Since capillary condensation enhances the sensing capabilities of a material, pore size distribution has been widely considered to be an important parameter in determining the sensitivity in a particular humidity range. Ideally, the membrane pore size should be comparable to r for enhanced sensing, e.g. $r = 10$ and 1.6 nm for 90% and 50% relative humidity levels, respectively.

The mechanism for nanoporous membrane humidity sensor is to sense the resistance and/or capacitance change of the nanosensors, which will be measured by interdigitated metal electrodes. The two equivalent circuit models [10] are shown in Fig. 2. The circuit in (a) is used when only high frequency semicircle is present and that in (b) is used where the low frequency spur co-exists with the high frequency semicircle. In Fig. 2a, only resistance R_1 and capacitance $C_1(\omega)$ change as water is absorbed, while in Fig. 2b, the fact that water ions can migrate toward the electrodes is also considered. In this paper, we only measure the dc resistance as a preliminary characterization of the sensors.

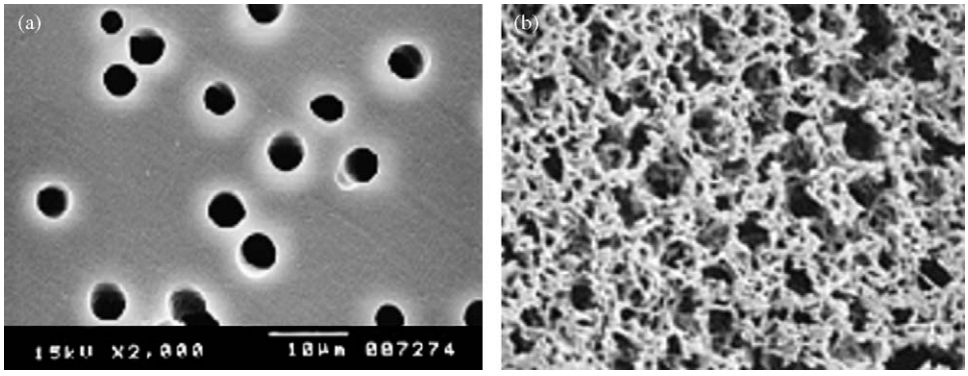

Fig. 1. SEM micrographs of the two nanoporous sensing materials: (a) polycarbonate and (b) polyester membranes.

Table 1
Properties of three nanoporous polymer membranes

Membrane material	Resistivity (Ω cm)	Dielectric constant at 1 MHz	Pore diameter (nm)	Pore density (pores/cm^8) or porosity	Thickness (μm)
Polycarbonate	5×10^{12}	5	200	3×10^8	10
Cellulose acetate	10^{14} to 10^{16}	2.9	200	66%	125
Nylon	10^{13}	3.4	100	55%	110

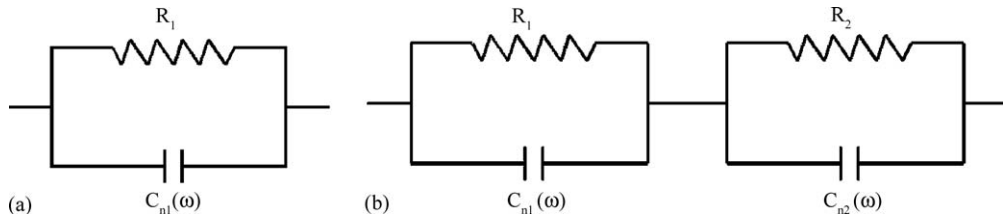

Fig. 2. Equivalent circuits used for fitting experimental data.

3. Design

The nanosensor is composed of a pair of interdigitated metal electrodes built on top of the porous layer for measuring the resistance or capacitance. The porous layer serves as the moisture-sensitive material. By changing the length of single electrodes, number of electrode pairs, and gap between adjacent electrodes, the design of the sensor can be optimized.

Five different electrode designs corresponding to two different fabrication methods are proposed. Designs A and B have relatively larger dimensions, as shown in Fig. 3, and are for the first fabrication method. In design A, there are four pairs of electrodes. The dimensions of electrodes are 10 mm × 0.5 mm and the gap between adjacent electrodes is 2 mm. In design B, there are five pairs of electrodes. The dimensions of a single electrode are 10 mm × 0.3 mm and the gap between two adjacent electrodes is 1 mm.

Designs C, D, and E, as shown in Figs. 4 and 5, have relatively smaller dimensions and are for the second fabrication method. In design C, there are 19 pairs of electrodes. The dimensions of electrodes are 13 mm × 0.5 mm with a 0.5 mm gap between electrodes. In design D, there are 9 pairs of electrodes, and the electrode fingers have different lengths. Both the width of a single electrode finger and the gap between adjacent fingers are 0.75 mm. The circular shape of design D sensors allows the maximum usage of sensing area in a single membrane compared with other designs. In design E, five sensors are arranged on a single 25 mm diameter membrane separately to compare their performances and to study the possibility to make a sensor array. All smaller sensors in design E have 9 pairs of electrodes, and have exactly the same shape but their dimensions are scaled. Although the dimensions are scaled to different size, these individual sensors in design E are expected to have the same nominal resistance because the membrane thickness is the same for all sensors. Another purpose of providing designs D and E is to demonstrate the fabrication flexibility of using various shadow masks, which are the silicon shadow mask and adhesive paper mask, respectively and will be discussed in more detail Section 4. With the silicon shadow masks, various sensors of flexible designs can be fabricated easily. In design E, sensor array with much smaller distance between electrodes and electrode width can be fabricated. We also believe there is some lower limit on the electrode distance and electrode width for the sensor fabrication. If the distance between electrodes or electrode width is too small, the sensor fabrication will be difficult and circuit-short between two adjacent electrodes may occur.

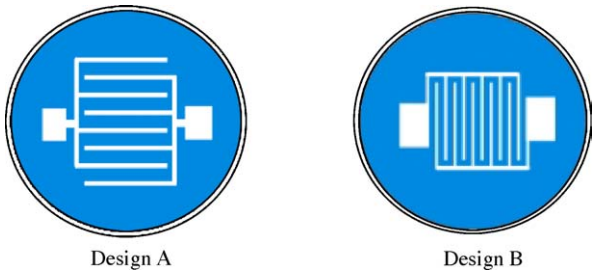

Fig. 3. Designs A and B type of humidity nanosensors (diameters are 25 mm for both designs).

4. Fabrication

Since acetone and photoresist developer react with the polymer substrate and make the sensing membrane inactive during photoresist stripping, conventional photolithography is not possible to fabricate the sensor electrodes. Therefore, two other methods were exploited using a shadow mask (or dry lift-off) technique.

The first method is to use an adhesive paper or sticky gel pack as a dry lift-off mask. The fabrication process is illustrated in Fig. 6. At first, the pattern of the electrodes was laid out using a CAD software (CorelDraw10) and the electrode patterns were printed on the adhesive paper or gel pack with an office printer. Then the electrode patterns were cut carefully with knife, and removed. Thus, a circular shadow mask with hollow electrode patterns was obtained. Then this shadow mask was attached to the sensing membrane. After sputtering the electrodes (50 Å Ti/1000 Å Au), the mask was removed with tweezers manually, leaving only the electrode patterns. The whole fabrication process took only several hours. This fabrication method works well for large electrode patterns. Fig. 7 shows two fabricated sensor photos.

In the second method, microfabricated silicon patterns were used as a shadow mask. Then the interdigitated electrodes were formed by sputtering through this mask on the polymer membrane. To prepare silicon patterns, conventional photolithography with deep reactive ion etching (DRIE) was used. Instead of making a chromium mask, a commercial high-resolution printer (3600 dpi) was used to

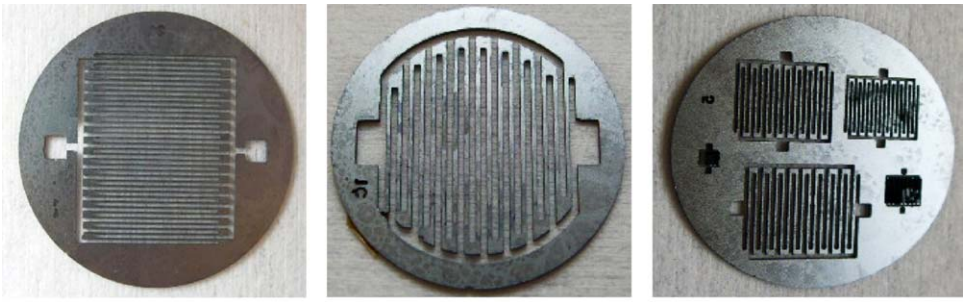

Fig. 4. Photos of the silicon shadow masks with electrode patterns fabricated by deep RIE process: designs C, D, and E from left to right, respectively (all silicon shadow masks are 26 mm in diameter).

print the electrode patterns on a transparency film. A 13 μm thick AZ4620 photoresist was spin-coated on the silicon wafer surface, and standard photolithography was used to pattern the shadow mask. It took about 6 h to deep-RIE etch through a 500 μm thick silicon wafer. Then, the silicon mask was put tightly on the polymer membrane, and gold was sputtered on the membrane with the K.J. Lesker Sputtering machine to fabricate the electrodes.

Silicon shadow mask is superior to adhesive paper and gel pack masks in the sense that the electrode feature sizes can be made much smaller and it is reusable. Same silicon shadow mask was used to fabricate sensors on different membranes for several times and it is observed that the silicon structures were still in good shape. After several gold sputtering runs, there will be a very thin gold film on the silicon shadow masks. This thin gold film can be easily removed with a gold etchant if necessary. Therefore it is a better method than using adhesive paper mask if high quantities of sensors are to be fabricated.

Once having the silicon shadow masks, one can fabricate tens of sensors within several hours without the need for cleanroom facilities. Therefore the proposed humidity nanosensors have the potential to compete with other sensors in terms of low-cost and quick fabrication.

5. Testing

Estimation and preliminary testing shows the resistances of the sensors are out of the range of conventional digital

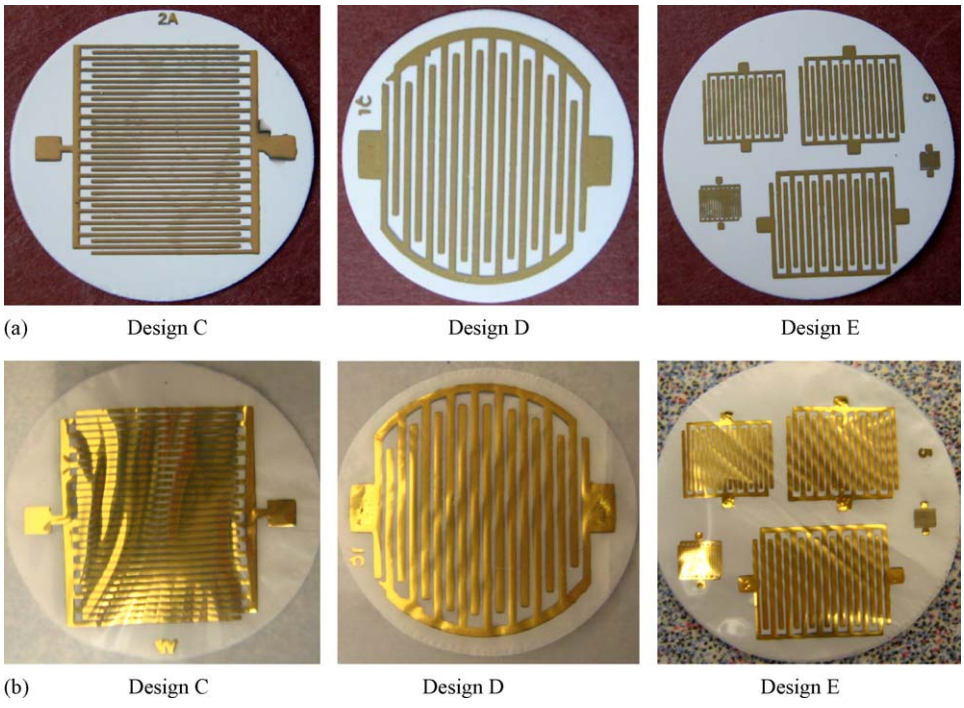

Fig. 5. (a) Photos of three nanosensors fabricated on nanoporous nylon membrane with silicon shadow masks, corresponding to designs C, D, and E (all membranes are 25 mm in diameter) and (b) photos of three nanosensors fabricated on nanoporous polycarbonate membrane with silicon shadow masks, corresponding to designs C, D, and E (all membranes are 25 mm in diameter).

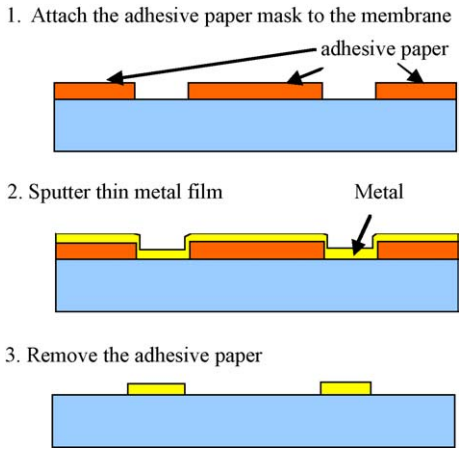

Fig. 6. Fabrication process of the humidity nanosensors using adhesive paper or gel pack as a shadow mask.

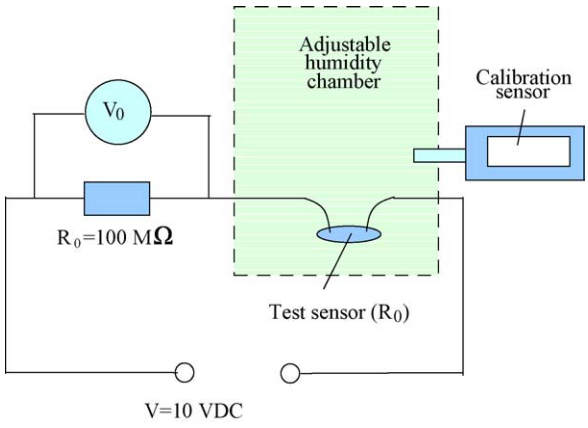

Fig. 8. Experimental test setup for the humidity sensors.

multimeters (usually 100 MΩ). So a simple voltage divider circuit was built to measure the dc resistance, as shown in Fig. 8. During testing interconnect wires were bonded to the sensors' bonding pads through silver paste. The sensor was hung inside a plastic humidity adjustment chamber without touching the wall of the chamber. A commercial humidity sensor (MicroDataLogger MDL03411) with a fast time response was used to monitor/adjust the chamber humidity. The sensor (R_s) was connected in series to a 100 MΩ resistor R_0. A 10 V dc was applied to both resistors, and V_0 (voltage along R_0) was measured by a multimeter (Agilent 34401A) with an input impedance larger than 10 GΩ. Therefore the resistance of the sensor is:

$$R_s = V_s \frac{R_0}{V_0} = (10 - V_0)\frac{R_0}{V_0}$$

Fig. 9 shows dc resistance versus relative humidity for design A and B devices fabricated on polycarbonate membranes at 25 °C. The resistance changes from 150 to 0.3 GΩ, and from 77 to 0.1 GΩ, for design A and B devices, respectively, while humidity changes from 39% to 100%. Design A device has larger resistance because it has less number of electrode pairs and larger gap between two adjacent electrodes than design B device.

Fig. 10 shows dc resistance versus relative humidity for three design C sensors fabricated on polycarbonate, cellu-

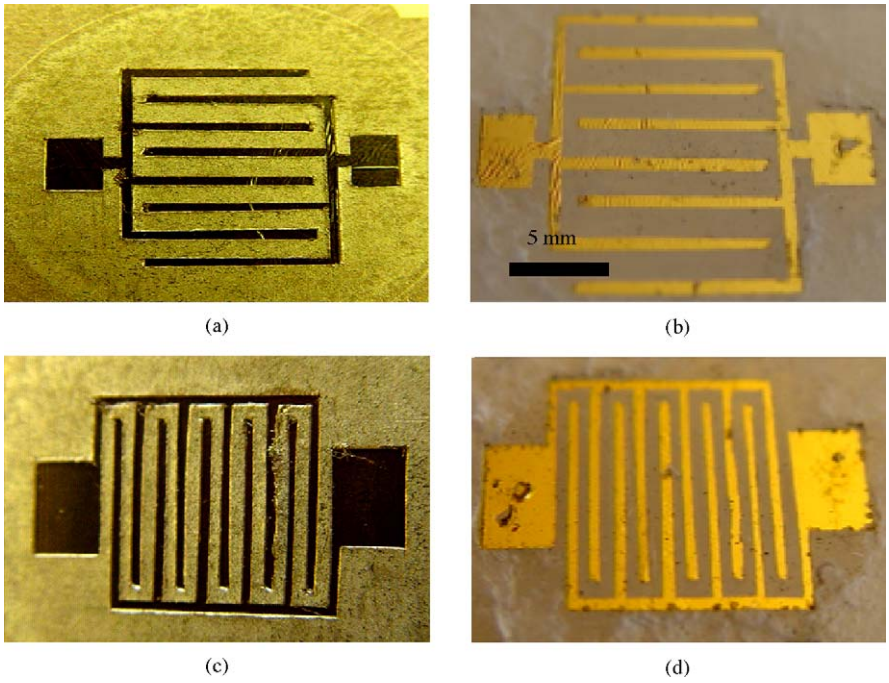

Fig. 7. Photos of the two humidity sensors fabricated on polycarbonate membranes with adhesive paper shadow masks: (a) design A sensor after sputtering before removing the paper mask, (b) design A device after removing the paper mask, (c) and (d) same as (a) and (b) but for a design B sensor.

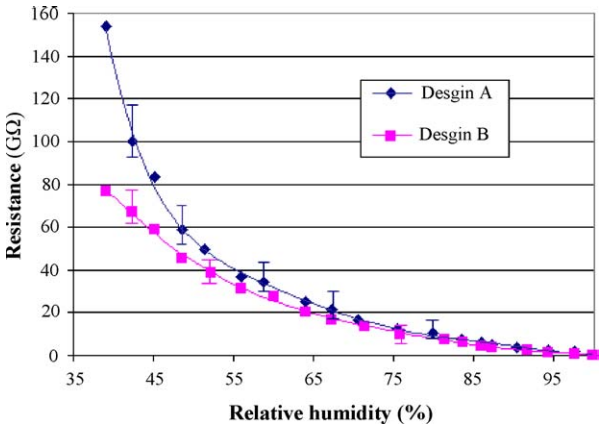

Fig. 9. The dc resistance measurements at 25 °C for various relative humidity values for design A and B devices fabricated on polycarbonate membranes.

lose acetate, and nylon membranes, respectively, at 25 °C. While relative humidity changes from 39% to 100%, the resistance changes from 300 to 2, 1612 to 26, and 1389 to 15 GΩ for polycarbonate, cellulose acetate, and nylon membranes, respectively.

Fig. 11 shows the time response of the three design C devices in Fig. 10 when they were taken out from a 100% to 39% relative humidity environment at 25 °C. It took about 4, 5, 8 min to get to steady state for the polycarbonate, cellulose acetate, nylon sensors, respectively.

Each sensor in Figs. 9–11 was tested two to three times, and the overall error during the testing is about 10–20%. The testing curves in Figs. 9–11 show the typical testing data conducted for each sensor. To better show the result, a fitted curve together with the error bars were used to show the testing results in Figs. 9–11. This demonstrates that the repeatability of the sensors is reasonably sufficient.

I–V curve of a design C sensor fabricated on polycarbonate membrane with silicon shadow mask has been measured by a HP 4155B Semiconductor Parameter Analyzer at room condition. Voltage applied to the sensor was switched from

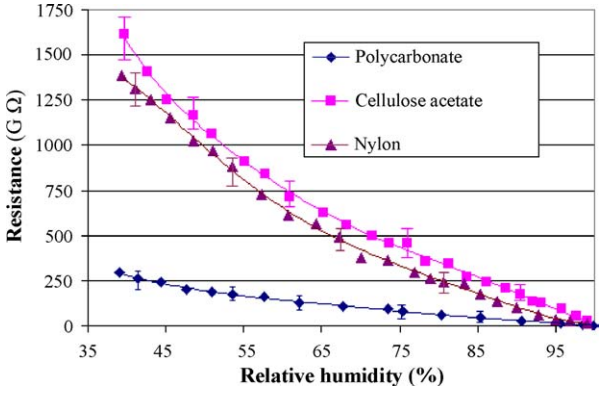

Fig. 10. The dc resistance measurements at 25 °C for various relative humidity values for three design C devices fabricated on polycarbonate, cellulose acetate, and nylon membranes, respectively.

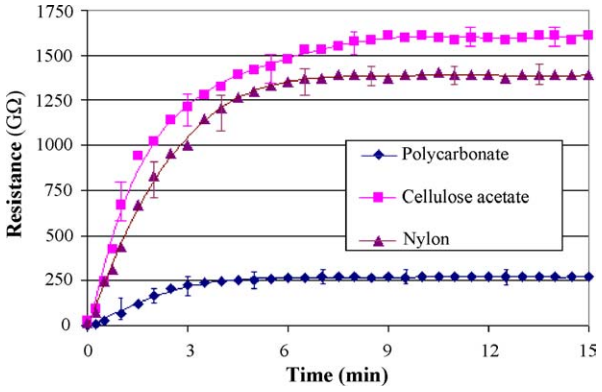

Fig. 11. Time response of the three design C devices (in Fig. 10) when they were taken out from 100% to 39% relative humidity environment at 25 °C.

−5 to +5 V and current was measured, as shown in Fig. 12. The curve shows that the sensor behaves generally ohmic, although there is some evidence for polarization and/or non-ohmic behavior. The resistance of the sensor was measured to be about 1300 GΩ which is very close to the estimated value of 1600 GΩ. The small difference between the estimated and the measured resistance may be arising from the distorted shape of the gold electrodes. As the sputtering process is performed, some gold goes underneath the silicon shadow mask resulting in a distorted electrode shape and this is not taken into account in the simulations.

Experiment results show that the nanosensor's resistance strongly depends on the fabrication and packaging method. During the electrode sputtering, gold may go underneath the silicon shadow mask, which can significantly change the total sensor resistance. Therefore even for the same sensor design with same type of membrane, the dc resistance may change a significant amount.

In addition, for design A and B sensors made with adhesive paper shadow mask on thin polycarbonate membranes, the thin membranes were bonded to a glass substrate with double-sided adhesive tapes in order to facilitate peeling off the shadow mask from the membrane after sputtering. The

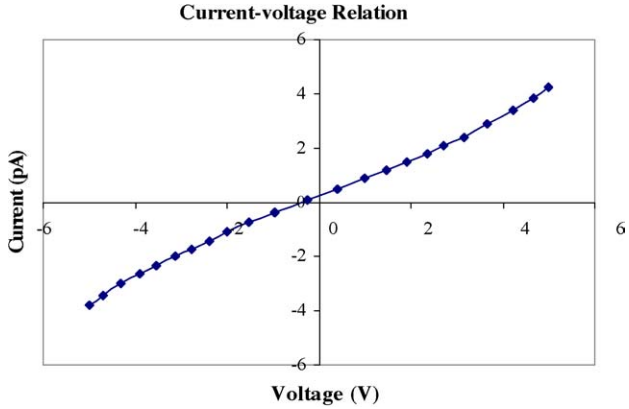

Fig. 12. *I–V* curve of a design C sensor fabricated on polycarbonate membrane.

tape may decrease the total resistance and lower the sensitivity. This probably explains why the measured resistance of design A and B sensors are smaller than that of design C device, although design A and B sensors should have larger design resistance by their dimensions. Also the adhesive paper mask may cause a decrease of the electrical resistivity of the humidity sensing membrane. Ideally, the sensor should be free from any substrate for best performance and uncertainties.

Testing of design D and most E sensors also shows good sensitivity of resistance change as humidity varies, although their nominal resistance is larger than design C. In design E, we expect the individual sensors of same shape but different size have the same nominal resistance since the membrane thickness are the same for all sensors. But testing result shows significant resistance difference for these individual sensors. This is possibly caused by the distorted electrode shape due to sputtering when the electrode distance of the sensors is small. We also noticed that some individual sensors in design E are electrode-shorted when the electrode width and the distance between electrodes is smaller than 150 μm. This may be the minimum size limit of the shadow mask fabrication method. The design D and E sensors that are not shorted generally have resistance about 4–10 times larger than design C. The working sensors generally have a nominal resistance about 4–10 times larger than design C. For improved sensor characterization, better testing equipments and/or better testing methods will be used in the future.

6. Modeling

Two-dimensional steady-state behavior of different nanosensor designs was modeled using the ANSYS® 7.0 software package. In the simulation, 0 and 1 V were applied to the two electrode pads, respectively. The volume resistivities of gold and polycarbonate used in the simulation were 2.21×10^{-8} and $5 \times 10^{10}\ \Omega\,m$, respectively. The voltage potential field and the electric current vector field were obtained. Fig. 13 shows the electric potential field and current density vector field of design A sensor. In addition, we calculated the dc resistance between the two electrodes.

The electric potential field and current density vector field shown in Fig. 13 are highly ordered between the adjacent electrode combs. The electric potential on each single electrode is almost the same, because the electric resistivity of gold is about 20 orders of magnitude smaller than that of polycarbonate membrane. Since the length of the electrodes is much larger than the gap between electrodes, the electric conduction between the two electrodes can be roughly taken as one-dimensional, which was confirmed by the ANSYS® 7.0 simulation result. Thus, a one-dimensional model can be used to estimate the resistance between the two electrodes.

With the electric resistivity listed above, the total resistance between the two electrodes was obtained as about

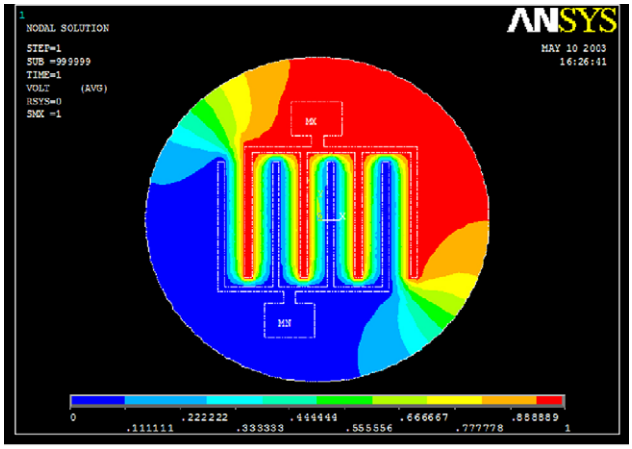

(a)

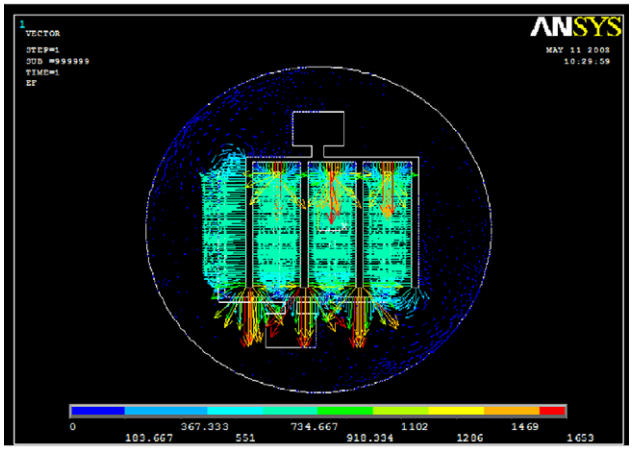

(b)

Fig. 13. Simulated electric potential field and current density vector field of design B nanosensor interdigitated electrodes fabricated on a polycarbonate membrane.

$1.38 \times 10^{14}\ \Omega$ for design A and $1.52 \times 10^{13}\ \Omega$ for design B, respectively using ANSYS® 7.0. These modeled resistances are very close to the theoretical results which are $1.43 \times 10^{14}\ \Omega$ for design A and $1.75 \times 10^{13}\ \Omega$ for design B, respectively, when taking the electric conduction one-dimensional.

The modeling resistance using nominal polymer resistivity differs from the measured resistance significantly. One possible explanation is that the actual resistivity of the porous membrane is much smaller than the resistivity used in the modeling. In real case, the membrane material is porous instead of bulk phase. There may already be a considerable amount of water vapor condensed inside the nanopores in ambient conditions, thus decreasing the nominal resistivity drastically. In addition, in design A and B sensors fabricated on thin polycarbonate membranes with adhesive paper shadow mask; we use a double-sided tape to bond the membrane to a glass wafer. This tape could increase the conductance of the sensors significantly.

7. Conclusions

Different designs of flexible and low-cost nanopore based polymer humidity nanosensors were proposed, and prototype sensors were successfully fabricated using two different methods: using an adhesive paper or a silicon mask with electrode patterns formed using DRIE as a shadow mask. An electrical circuit was designed to measure the dc resistance of the fabricated sensors. Among the tested designs, design B sensor exhibit the lowest sensitivity value of 1.3 GΩ/% RH and it still is three orders of magnitude higher than the maximum sensitivity achieved for both ceramic [2], nanoporous alumina [8], and nanoporous silicon [1] based humidity sensors. Testing results showed that the dc resistance between electrodes for design A, B and C sensors changes with very high sensitivity and monotonically as the relatively humidity changes from 39% to 100%. It takes about 4–8 min for the resistance to reach steady state when the sensor was taken from 100% to 39% relative humidity at the room temperature. This speed is reasonable for low response time applications. These results showed the feasibility of the preliminary designs of compliant and low-cost nanopore polymer membrane based humidity nanosensors. Moreover, simulations were conducted to estimate the electric resistance between the electrodes for an optimal electrode pattern design. The electric potential field and electric current density vector field were obtained and analyzed. In the future, the whole sensor would be miniaturized with the detection electronics and an array of these sensors would be fabricated as flexible sheets with an integrated wireless communication unit on them. Thus, these easy to implement and flexible sheets would enable in situ humidity mapping of complex and vulnerable three-dimensional surfaces such as roofs or airplane bodies. Hence, possible applications include water leakage detection and mapping on roofs and in situ humidity measurements on airplane surfaces.

Acknowledgements

The authors would like to thank Prof. David W. Greve for helping on the sensor characterization. This work was funded by The Pennsylvania Infrastructure Technology Alliance (PITA) Program, Institute of Complex Engineering Systems at the Carnegie Mellon University.

References

[1] D.K. An, L.H. Mai, Surface effect humidity sensor based on alumina and porous silicon materials: some electrical parameters, sensitivity and internal noises in comparison, Proc. IEEE Sensors 1 (2002) 633–640.
[2] T. Nitta, S. Hayakama, Ceramic humidity sensors, IEEE Trans. Components Hybrids Manuf. Technol. 3 (1980) 237–243.
[3] S.J. Kim, J.Y. Park, S.H. Lee, S.H. Yi, Humidity sensors using porous silicon layer with mesa structure, J. Phys. D: Appl. Phys. 33 (2000) 1781–1784.
[4] L.J. Golonka, B.W. Licznerski, K. Nitsch, H. Teterycz, Thick-film humidity sensors, Meas. Sci. Technol. 8 (1997) 92–98.
[5] J.J. Steele, K.D. Harris, M.J. Brett, Nanostructured oxide films for high-speed humidity sensors, Mater. Res. Soc. Symp. Proc. 788 (2004) L11.4.1–L11.4.6.
[6] E.J. Connoly, P.J. French, Relative humidity sensors based on porous polysilicon and porous silicon carbide, Proc. IEEE Sensors 1 (2002) 499–502.
[7] G.M. O'Halloran, P.M. Sarro, J. Groeneweg, P.J. French, A bulk micromachined humidity sensor based on porous silicon, in: Proceedings of the Transducers, Chicago, USA, June 16–19, 1997.
[8] O.K. Varghese, D. Gong, M. Paulose, K.G. Ong, C.A. Grimes, E.C. Dickey, Highly ordered nanoporous alumina films: effect of pore size and uniformity on sensing performance, J. Mater. Res. 17 (2002) 1162–1171.
[9] A. Wu, M.J. Brett, Sensing humidity using nano-structured SiO posts: mechanism and optimization, Sens. Mater. 13 (7) (2001) 399–431.
[10] E.C. Dickey, O.K. Varghese, K.G. Ong, et al., Room temperature ammonia and humidity sensing using highly ordered nanoporous alumina films, Sensors 2 (2002) 91–110.
[11] H. Shibata, M. Ito, M. Asakursa, K. Watanabe, A digital hygrometer using a polyimide film relative humidity sensor, IEEE Trans. Instrum. Meas. 45 (1996) 564–569.
[12] M. Dokmeci, K. Najafi, A high-sensitivity polyimide capacitive relative humidity sensor for monitoring anodically bonded hermetic micropackages, J. Microelectromech. Syst. 10 (2001) 197–204.
[13] C. Laville, C. Pellet, Comparison of three humidity sensors for a pulmonary function diagnosis microsystem, IEEE Sensors J. 2 (2002) 96–101.
[14] C. Laville, C. Pellet, Interdigitated humidity sensors for a portable clinical microsystem, IEEE Trans. Biomed. Eng. 49 (2002) 1162–1167.
[15] C.Y. Lee, G.B. Lee, Micromachine-based humidity sensors with integrated temperature sensors for signal drift compensation, J. Micromech. Microeng. 13 (2003) 620–627.
[16] U. Kang, K.D. Wise, A high-speed capacitive humidity sensor with on-chip thermal reset, IEEE Trans. Electron Devices 47 (2000) 702–710.
[17] Y.L. Yang, L.H. Lo, et al., Improvement of polyimide capacitive humidity sensor by reactive ion etching and novel electrode design, Proc. IEEE Sensors 1 (2002) 511–514.

Biographies

Bozhi Yang received the B.S. degree from Xi'an Jiaotong University in 1997 and the M.S. degree from Tsinghua University in 2000, respectively. He has been studying towards his Ph.D. degree in mechanical engineering at Carnegie Mellon University, Pittsburgh, PA since 2001, where his research is on the development of novel micro flow control devices for biomedical applications. His other research effort includes modeling of microfluidic devices, developing integrated MEMS sensors for biophysical characterization, and developing surface-tension based microfluidic devices for microdialysis.

Qiao Lin received the Ph.D. degree in mechanical engineering from the California Institute of Technology (Caltech), Pasadena, in 1998 with dissertation research on kinematics and mechanics of robotic manipulation. He conducted postdoctoral research in Microelectromechanical systems (MEMS) at the Caltech Micromachining Laboratory from 1998 to 2000, and has since been an Assistant Professor in the Department of Mechanical Engineering at Carnegie Mellon University, Pittsburgh, PA. His research interests are in MEMS, including analysis, design and fabrication of micro/nano-fluidic, thermal, and robotic devices for biological and chemical applications.

Metin Sitti received the B.Sc. and M.Sc. degrees in electrical and electronics engineering from Bogazici University, Istanbul, Turkey, in 1992 and 1994, respectively, and the Ph.D. degree in electrical engineering from the University of Tokyo, Tokyo, Japan, in 1999. He was a research scientist and lecturer in the Department of Electrical Engineering and Computer Sciences, University of California at Berkeley during 1999–2002, working in micromechanical flying insects and biomimetic gecko adhesives projects, and teaching the graduate level new Micro/Nano-Robotics course. He is currently an assistant professor and the director of the NanoRobotics Laboratory in Department of Mechanical Engineering at the Carnegie Mellon University. His research interests include micro/nanorobotics, micro/nanomanufacturing, MEMS/NEMS, and biomedical micro/nanotechnology. He received the NSF CAREER award in 2005, and the Struminger award for micro/nanoengineering teaching activities at CMU. He also received the best paper award in the IEEE Robotics and Biomimetics Conference (2004), the best paper award in the IEEE/RSJ International Conference on Intelligent Robots and Systems (1998), and the best video award (2002) in the IEEE Robotics and Automation Conference. He is the chair of the IEEE Nanotechnology Council, Nanorobotics and Nanomanufacturing Technical Committee and the IEEE Robotics and Automation Society, Rapid Prototyping in Robotics and Automation Technical Committee.